Enhanced Tribocorrosion Performance of Cr/GLC Multilayered Films for Marine Protective Application

Lei Li,[†,‡,§] Lin-Lin Liu,[†,§] Xiaowei Li,[†] Peng Guo,[†] Peiling Ke,[*,†] and Aiying Wang[*,†]

[†]Key Laboratory of Marine Materials and Related Technologies, Zhejiang Key Laboratory of Marine Materials and Protective Technologies, Ningbo Institute of Materials Technology and Engineering, Chinese Academy of Sciences, Ningbo 315201, China

[‡]University of Chinese Academy of Sciences, Beijing 100049, China

S *Supporting Information*
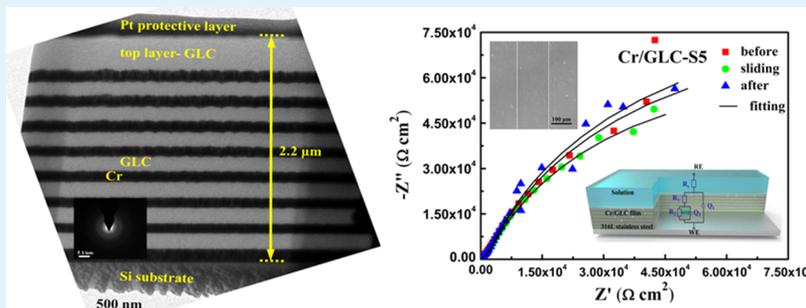
ABSTRACT: The corrosion and tribology are all closely related to the interface/surface of materials, which are extremely important for the mechanical components used in harsh marine environments. In this work, we fabricated Cr/graphite-like carbon (GLC) multilayered films with different modulation periods on the 316L stainless steels by direct current magnetron sputtering. Tribocorrosion tests in artificial seawater show that the tribocorrosion resistance of the Cr/GLC films is improved as the modulation period decreases from 1000 to 333 nm and then drastically drops with further decreasing to 250 nm. By taking a top-layer thickening strategy for the Cr/GLC film with 250 nm modulation period, the tribocorrosion performance is significantly enhanced. The corresponded mechanisms are discussed in terms of the film structure and electrochemical corrosion behavior.

KEYWORDS: Cr/GLC films, multilayered, tribocorrosion, artificial seawater

1. INTRODUCTION

Over the past couple of decades, marine industries have been rapidly developed in the world. In particular, with strong demands of environment-friendly and energy-saving technology, it is of great importance to enhance the comprehensive properties of frictional components in marine systems. Some marine frictional components suffer mechanical wear and corrosion attack simultaneously in aggressive marine environments, where the safety and service lifetime of these components are strongly dependent on the constituent material performance under marine tribocorrosion.[1] In general, tribocorrosion is defined as the chemical−mechanical process leading to a degradation of a material exposed to an aggressive environment with a tribological contact. It can bring the destruction and remove of the passive film and thus increase the area directly exposed to corrosive solution, resulting in accelerated corrosion and wear.[2−7] More importantly, the synergistic effect of corrosion and wear can substantially accelerate the material degradation and the mass loss.[8] Stainless steel, a popular marine material, is widely used as structural components in marine engineering because of its exceptional corrosion resistance, good weldability, and fabricability. However, the inferior tribocorrosion properties will severely

endanger the operation performance of the frictional components of marine equipment.[9−11] One of the practicable strategies to enhance the tribocorrosion resistance of metal components is to fabricate functional coatings with combined good lubrication and corrosion protective ability.

Amorphous carbon (a-C) films, consisting of sp^3- and sp^2-bonded structures, can be divided into diamond-like carbon (DLC) and graphite-like carbon (GLC) films. GLC films have attracted much attention from the science community and industrial field in the past few decades owing to their desirable properties including chemical inertness, high hardness, and low friction coefficient, as well as the facile deposition methods.[12−16] However, the inadequate adhesion strength often leads to the deposited carbon film flaking or peeling off from the substrate, thus suffering poor long-term tribological properties.[17,18] Moreover, through-thickness defects with pinholes formed in the physical vapor deposition process usually give rise to the inward penetration of corrosive species (e.g., Cl^- and SO_4^{2-}) toward the substrate, resulting in the

deteriorative corrosion resistance.[19] Interlayer addition[19−22] and multilayer structure design[19,23−27] were attempted to solve the above tribological and corrosion problems of carbon film coated substrate. He et al.[20] systematically investigated the tribological behavior of DLC-coated AISI 52100 steel in different testing styles. They found that by means of a dynamic atomic mixing in interface, the metallic intermediate layer (e.g., Cr and Mo) greatly enhanced the interfacial adhesion and tremendously improved the wear resistance of DLC films. Zhang et al.[24] compared the tribological behaviors of monolayered and multilayered DLC films in dry conditions and found that the multilayered structure had little influence on friction coefficient but significantly reduced the wear rate. Bai et al.[23] studied the corrosion and tribocorrosion performances of a-C coated Ti6Al4V alloy in Hank's solution. They confirmed that a-C multilayer films exhibited enhanced corrosion and wear resistance compared to the single-layer film. For the interlayer and multilayer design of a-C film, the interlayer choice and the multilayer structural parameter (e.g., modulation period and modulation ratio) are crucial factors determining the protective performances of amorphous carbon film to the substrate. In recent work, Wang et al.[28] showed that a Cr intermediate layer can both improve adhesion strength and tribological performance of the GLC film, which is consistent with previous studies by Stallard et al.,[29] where high load-bearing capacity accompanied with low friction and wear under three environments (air, oil, and water) was observed.

In this paper, a series of Cr/GLC multilayered films are fabricated by dc magnetron sputtering on 316L stainless steel. The role of modulation period on the tribocorrosion behavior of deposited Cr/GLC films is focused in artificial seawater. The related mechanism is discussed in terms of the structure and tribological and electrochemical corrosion behaviors of films. Eventually, the Cr/GLC film with 250 nm modulation period is optimized together with a top-layer thickening design to obtain superior tribocorrosion resistance. The results bring forward a new concept to fabricate tribocorrosion-protective coating materials for marine mechanical components in harsh environments.

2. EXPERIMENTAL SECTION

2.1. Film Preparation. A direct current magnetron sputtering technique was used to fabricate the Cr/GLC multilayered films. P-type (1 0 0) Si wafers and mirror polished 316L stainless steels with dimensions of 30 mm × 20 mm × 28 mm were used to deposit the films as substrates separately. The Si wafers and 316L stainless steels were cleaned in acetone, ethanol in sequence and dried with a hair dryer. The distance from the substrates to the targets was 10 cm. The base pressure in the chamber was 4.0×10^{-3} Pa. All substrates were etched and precleaned in Ar^+ plasma glow with substrate bias voltages of −350 V for 30 min. During the film deposition process, the Ar gas was introduced to sputtering target in a flow rate of 50 sccm. A Cr buffer layer was first deposited with a target current 3.0 A and a bias voltage −100 V. Deposition of the GLC layer was kept under a target current of 3.0 A and a bias voltage of −200 V with a high purity graphite target (99.99%). Cr/GLC films with different modulation periods were obtained by commutative deposition of Cr layers and GLC layers. The deposition procedures of Cr and GLC films were set as one block. The block was repeated from two to eight times to form Cr/GLC multilayered films. Specific deposition parameters were shown in Table 1.

2.2. Microstructure Characterization. The cross-sectional and wear track morphologies of the Cr/GLC multilayered films were observed by field emission scanning electron microscopy (SEM, FEI Quanta FEG 250) equipped with energy dispersive spectroscopy

Table 1. Deposition Parameters of the Cr/GLC Multilayered Films

samples	modulation period (nm)	deposition time of Cr buffer layer (min)	deposition time of GLC layer (min)
Cr/GLC-S1	1000	11	100
Cr/GLC-S2	500	6	50
Cr/GLC-S3	333	4	33
Cr/GLC-S4	250	3	22

(Oxford X-Max). Microstructure and atomic bond of GLC films were analyzed by Raman spectroscopy (inVia Reflex, Renishaw) with a 532 nm laser. To characterize the hardness and elastic modulus of the films, a nanoindenter (Nano Indenter, MTS Ltd, USA) was used. The representative hardness of the film was selected in the depth of 200 nm to avoid the effect caused by the substrate. The cross-sectional microstructure of the Cr/GLC films was measured by high-resolution transmission electron microscopy (TEM) (FEI Tecnai F20). The film composition was analyzed by radio frequency glow discharge optical emission spectrometry (RF-GD-OES, GDA 750HP). The surfaces of the Cr/GLC films were etched by an Ar^+ ion beam of 2 kV before the measurement.

2.3. Tribocorrosion and Electrochemical Corrosion Tests. Tribocorrosion behaviors of the Cr/GLC films in artificial seawater were evaluated by a linear reciprocating tribometer (RTEC MFT5000) integrated with a three-electrode electrochemical system. The schematic diagram of the tribocorrosion setup is shown in Figure 1.
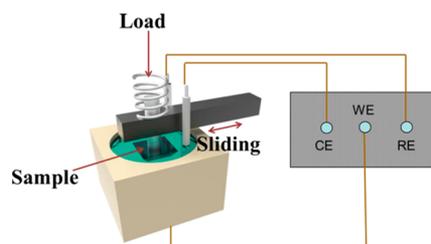
Figure 1. Schematic diagram of the tribocorrosion setup.

A commercial Si_3N_4 ball with diameter 6 mm was chosen as the sliding counterpart because of its high hardness and anticorrosion properties. The applied normal load was 5.0 N which was coincident with a maximum initial Hertzian contact pressure of about 1.14 GPa. The employed electrolyte was artificial seawater, which was prepared on the basis of the standard ASTM 1141-98 as shown in Table 2.[30] The sliding velocity and frequency were set as 0.02 m/s and 2 Hz, respectively. The total test time was 60 min. After the tribocorrosion tests, the section profiles of wear tracks were measured by using a surface profilometer (Alpha-Step-IQ). The wear rate was calculated by using the following equation:

$$W = V/(F \times L) \tag{1}$$

where V, F, and L are the wear loss in mm^3, applied normal load in N, and the total sliding distance in m.[31]

The electrochemical measurements were performed on a ModuLab (Solartron Analytical) electrochemical workstation by a conventional three-electrode electrochemical cell, which contains samples with an exposed area of 3 cm^2 serving as the working electrode, a saturated calomel working as the reference electrode, and a platinum plate as the counter electrode. Experiments were carried out at ambient temperature (25 ± 1 °C) in artificial seawater. All potentials in this paper were measured by a saturated calomel electrode, which had a more positive potential of 0.242 V than the standard hydrogen electrode. Tribocorrosion tests were conducted under open circuit potential (OCP) condition, and evolution of OCP was recorded. Potentiodynamic measurements were initiated after a steady OCP. The potential was from −0.7 to 1.3 V at a sweep rate of 2 mV/s. Tribocorrosion tests were conducted under protective potential condition in potentiostatic

Table 2. Chemical Composition of Artificial Seawater (g/L)

constituent	NaCl	MgCl$_2$	Na$_2$SO$_4$	CaCl$_2$	KCl	NaHCO$_3$	KBr	H$_3$BO$_3$	SrCl$_2$	NaF
concentration	24.53	5.20	4.09	1.16	0.695	0.201	0.101	0.027	0.025	0.003

tests, and a selected protective potential was applied on the Cr/GLC film. Other experimental conditions, such as the sliding setup, are the same as the tribocorrosion tests conducted under OCP condition. The electrochemical impedance spectroscopy (EIS) technique was used to evaluate the corrosion properties of Cr/GLC multilayered films before, during, and after tribocorrosion. The EIS measurements were registered at OCP in the frequency range of 10^5 to 10^{-2} Hz with 10 mV sinusoidal perturbation. The experimental EIS data were analyzed with the ZSimpWin software package and modeled by the proper electrical equivalent circuit. Mott–Schottky analysis was employed to evaluate the electric characteristics of the Cr/GLC multilayered films, which was performed at a frequency of 1.0 kHz applying a sinusoidal ac perturbation of 10 mV and displacing the potential from 0.2 to −0.8 V in 25 mV decrement. All of the electrochemical tests were conducted three times for checking the repeatability.

For comparison, the corresponding tribocorrosion and EIS measurements were also conducted on the 316L stainless steel substrate.

3. RESULTS AND DISCUSSION

3.1. Film Characterization. Figure 2 shows the back-scattered electron images of cross-sectional microstructure of
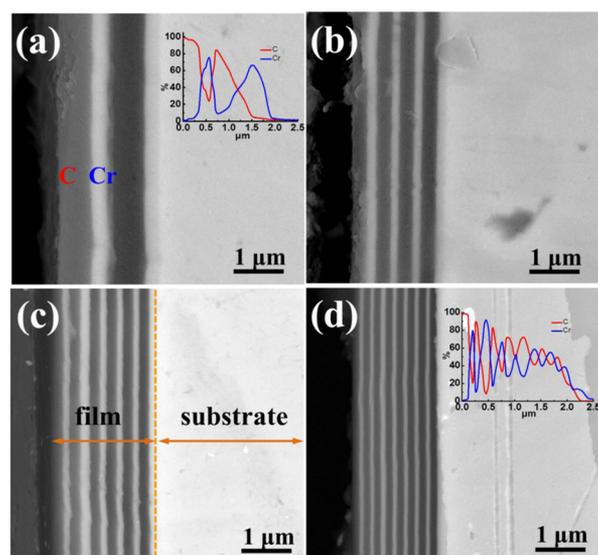
Figure 2. Cross-sectional morphologies and GD-OES profile analysis of Cr/GLC multilayered films with different modulation periods. (a) Cr/GLC-S1, (b) Cr/GLC-S2, (c) Cr/GLC-S3, and (d) Cr/GLC-S4.

the Cr/GLC multilayered films. These films exhibit cyclical layer structure and have an overall thickness of ~2.0 μm. All of them are composed of the Cr interlayer (bright part in Figure 2) and GLC layer (dark gray part in Figure 2), and they present clear interface and good bond to the substrate, indicating that the structure and modulation period can be accurately controlled. The thickness of top-layer amorphous carbon films decreases from 750 to 180 nm with the decrease of the modulation period. All the films have the same modulation ratio (the thickness ratio of Cr and GLC is 1:2.5 ≈ 1:3.0). Insets in Figure 2a,d are the composition depth profiles of elements in Cr/GLC multilayered films (taking the films with S1 and S4 as examples) by GD-OES measurement. Obviously, the depth distribution shows clearly elemental distribution between the alternative Cr and GLC layers, agreeing well with the multilayered structure of the Cr/GLC films characterized by SEM. However, it can be noted that the elemental distribution in the film/substrate interface partly deviates from the periodic structure observed by SEM, which is mainly ascribed to the substrate effect.

Raman spectroscopy is an effective tool to elucidate the atomic bond of amorphous carbon films. Figure 3a shows the Raman spectra of Cr/GLC multilayered films with different modulation periods. All of the Raman spectra present a typical broad characteristic of amorphous carbon in the wavelength from 800 to 2000 cm^{-1}. The broad peak can be designated to D peak at ~1380 cm^{-1} and G peak at ~1552 cm^{-1}.[32] These two peaks are closely related to the carbon sp^2 structure, where the G peak is originated from stretching mode of sp^2 atoms, while the D peak is due to the breathing mode.[33] Empirically, it is known that the content of the sp^2 hybridization bond in the film increases as the position of G peak shifts upward, and the intensity ratio of D peak to G peak (I_D/I_G) decreases with the decrease of sp^2 cluster size. Figure 3b illustrates the fitted G peak position and I_D/I_G. Both the G peak and I_D/I_G ratio vary in a small range of 1552 ± 1 cm^{-1} and 3.13 ± 0.04, as the modulation period of the Cr/GLC film decrease from 1000 to 250 nm. This reveals that the atomic bond structure of the GLC layer has no significantly change with the variation of the modulation period of the Cr/GLC film.

3.2. Mechanical Properties. The mechanical properties of Cr/GLC multilayered films with different modulation periods were characterized, as shown in Figure 4. In Figure 4, the hardness (H) of Cr/GLC multilayered film increases with the
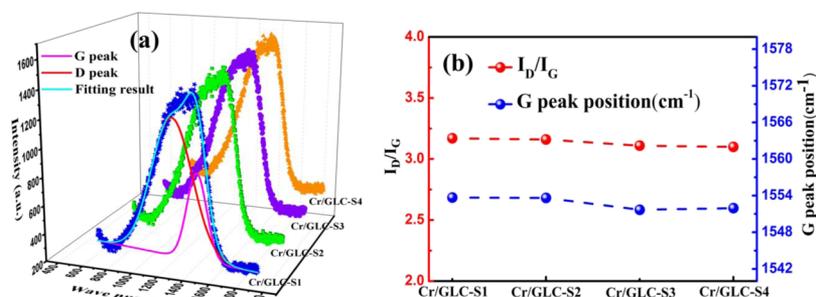
Figure 3. (a) Raman spectra and (b) fitted G peak position, I_D/I_G of Cr/GLC multilayered films with different modulation periods.
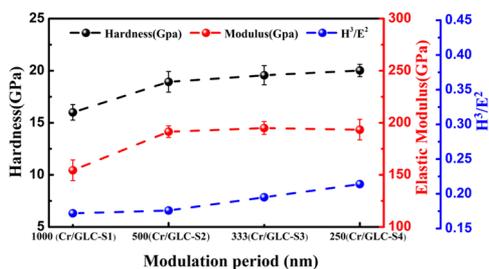
Figure 4. Mechanical properties of Cr/GLC multilayered films with different modulation periods.

decreasing modulation period. A maximum hardness of 20.03 ± 0.59 GPa is achieved for the Cr/GLC-S4 film with a 250 nm bilayer thickness. Similar dependence of the hardness of multilayered films on the modulation period has been reported by previous studies.[34−36] The hardness enhancement with the decrease in the bilayer period is a typical feature of multilayered coatings, which is mainly ascribed to the dislocation blocking and the alternating-stress strengthening at interfaces.[37,38] The elastic modulus (E) of the Cr/GLC multilayered film increases from 154.35 ± 9.87 to 191.44 ± 5.55 GPa with decreasing the modulation period from 1000 to 500 nm and then levels off around 193 GPa, as the modulation period is further reduced. It is well-known that the high hardness of the film is not absolutely related to a good wear resistance, and the ductility (inversely of elastic modulus) is also simultaneously considered. The ratio of H^3/E^2 representing plastic deformation resistance can be served as a parameter to assess the tribological property of the film.[39,40] As shown in Figure 4, the evolution of the H^3/E^2 value with modulation period shows a trend similar to that of hardness, implying that the plastic deformation resistance of the Cr/GLC multilayered films continuously increases with the modulation period ranged from 1000 to 250 nm. As such, it may be inferred that the tribological performance of the Cr/GLC multilayered films can be improved by increasing modulation number.

3.3. Friction and Wear. Figure 5 shows the typical friction coefficient curves of Cr/GLC multilayered films sliding against

Figure 5. Friction coefficient curves of Cr/GLC multilayered films sliding against Si$_3$N$_4$ balls in artificial seawater.

Si$_3$N$_4$ balls under tribocorrosion conditions. Clearly, the Cr/GLC multilayered films with relatively large modulation period, namely S1, S2, and S3, present a similar tribological behavior, and their friction curves can be characterized by two different stages: (1) an initial decrease from a high value to 0.075 within 100 s and (2) a subsequent and gradual increase to a relatively steady state stage with minor fluctuations. Contrarily, for the Cr/GLC-S4 film, following a low and quasistable friction stage

in initial 200 s, a drastic increase in the friction coefficient is observed. For further assessing the influence of the modulation period on the tribocorrosion behaviors, the average friction coefficients and wear rates of the Cr/GLC multilayered films are summarized in the histogram illustrated in Figure 6.

In Figure 6a, the average friction coefficients of Cr/GLC multilayered films range from 0.063 to 0.055 (from S1 to S3), reflecting their outstanding self-lubricating behaviors in artificial seawater. A cathodic protection potential, −0.4 V versus. OCP (see Figure S1 in Supporting Information for the potentiodynamic polarization curves of Cr/GLC multilayered films), was applied to make sure the effect of pure mechanical wear on the total material loss.[41] The corrosion effect on the total material loss of samples in the tribocorrosion test with cathodic protection is neglectful,[5,42] namely, pure mechanical wear is considered. Also, it can be found that friction coefficients of Cr/GLC multilayered films under pure mechanical wear conditions range from 0.058 to 0.043 (from S1 to S3) in artificial seawater, which is lower than those under tribocorrosion conditions. On the other hand, the Cr/GLC-S4 multilayered film in the tribocorrosion test with and without cathodic protection both is totally worn out, which results from the fact that the thinner top amorphous carbon functional layer cannot resist the synergistic effect of wear and corrosion or simplex mechanical friction effect, finally resulting in the enhanced wear rate. Total wear rates and wear rate ratios of pure mechanical wear and tribocorrosion are shown in Table 3. It can be seen that, expect for Cr/GLC-S4, the tribocorrosion properties of other Cr/GLC multilayered films are improved with the decrease of the modulation period, and the mechanical wear is predominantly responsible for the total material loss under tribocorrosion condition.[41] The current evolution curves of the Cr/GLC multilayered films under cathodic protection condition are provided as Supporting Information in Figure S2. Moreover, the total tribocorrosion volume loss (K_{wc}) is subdivided as follows:[43−45]

$$K_{wc} = K_{wo} + \Delta K_{wc} + K_{co} + \Delta K_{cw} \qquad (2)$$

where K_{wo} is the material loss caused by mechanical wear without the effect of corrosion, ΔK_{wc} is the increased material loss resulting from the corrosion accelerating wear rate, K_{co} is the material loss caused by corrosion without the effect of wear, and ΔK_{cw} is the increased corrosion rate because of wear. Generally, K_{co} was always very small,[46] and thus, eq 2 can be simplified as follows:

$$K_{wc} - K_{wo} \approx \Delta K_{wc} + \Delta K_{cw} \qquad (3)$$

The specific percentages of the synergistic effect are shown in Table 3.

The wear track morphologies of Cr/GLC multilayered films after the tribocorrosion test are shown in Figure 7. Obviously, the exfoliation areas are observed on the surface of wear tracks, indicating that the material loss of Cr/GLC multilayered films under tribocorrosion condition might result from local film peeling from the substrate. As shown in Figure 7a,d, the serious film delamination occurs in the Cr/GLC-S1 and Cr/GLC-S4 multilayered films; especially for the latter, a number of ploughed grooves also come out in the wear track. In consequence, the local delamination is a main factor to the durability of the Cr/GLC multilayered film in artificial seawater on account of its great influence on tribocorrosion failure. When the Cr/GLC films are sliding with Si$_3$N$_4$ balls in artificial seawater, the film defects may extend below the sliding surface.
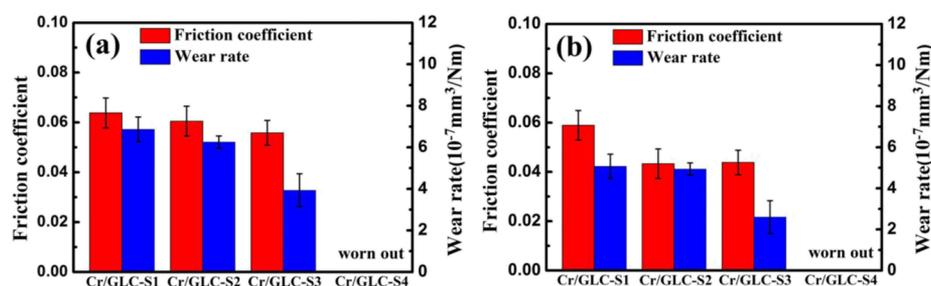
Figure 6. Average friction coefficients and wear rates of Cr/GLC multilayered films. (a) Tribocorrosion conditions and (b) cathodic protection conditions.

Table 3. Summary of Material Loss Components for the Cr/GLC Multilayered Films with Different Modulation Periods

samples	total wear rate (10^{-7} mm^3/Nm)	pure wear rate (10^{-7} mm^3/Nm)	ratio (pure wear/total wear) (%)	ratio (synergistic effect/total wear) (%)
Cr/GLC-S1	6.86	5.07	74	26
Cr/GLC-S2	6.25	4.94	79	21
Cr/GLC-S3	3.93	2.60	67	33
Cr/GLC-S4				
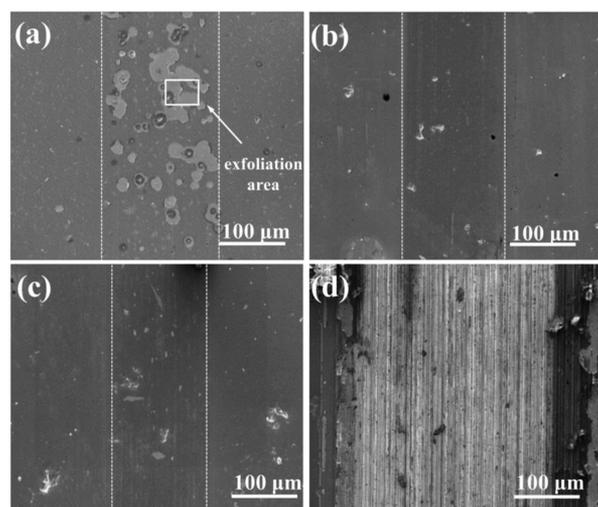
Figure 7. SEM morphologies of wear track of Cr/GLC multilayered films after the tribocorrosion test. (a) Cr/GLC-S1, (b) Cr/GLC-S2, (c) Cr/GLC-S3, and (d) Cr/GLC-S4.

The formation of through-hole by defect extension provides the channel of aggressive anion. Under a few rounds of reciprocating sliding, seawater can infiltrate into these defects. The 316L SS substrate near the defects is activated, and the Cl$^-$ ions can accelerate the dissolution of atoms in seawater.[47] Finally, the bond strength of film-substrate is seriously weakened.[48] The electrochemical reaction via electron exchange leads to the substrate material loss. Furthermore, the flaking of the Cr/GLC multilayered films will be intensified by wedging function from seawater penetrating into the defects. Eventually, the synergistic effect of wear and corrosion can substantially accelerate the tribocorrosion failure. With the decrease of modulation period, the exfoliation area shrinks, which is ascribed to the fact that the multilayer structure prevents the formation of through-hole and limits the defect propagation. Unexpectedly, the Cr/GLC-S4 film completely peels from the substrate in combining effect of corrosion and wear, which is ascribed to the thinner top layer amorphous carbon. The corresponding mechanism will be discussed in section 3.5. Also, the graphitization effect of tribofilms on the

surface in contact could bring down the friction and wear rate during the tribotest. Raman spectra obtained from the tribofilms transferred on Si$_3$N$_4$ balls are shown in Figure S3.

3.4. OCP and EIS Analysis. The OCP evolution is directly related to the electrochemical status of the electrode surface under tribocorrosion solicitations and can give a qualitative information of the surface electrochemical reactivity.[49,50] Figure 8 shows the evolution of the OCP over time before, during, and
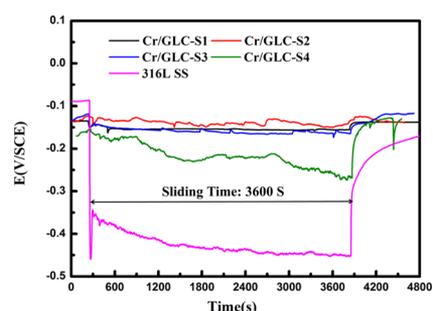
Figure 8. Evolution of OCP with time for Cr/GLC multilayered films and 316L stainless steel in the tribocorrosion test.

after the tribocorrosion test for the four Cr/GLC multilayered films and uncoated 316L stainless steel. As shown, a sharp negative shift in the OCP is observed for the 316L stainless steel at the beginning of the tribocorrosion test, reflecting an activation of the worn surface as a consequence of the mechanical wear. This behavior is attributed to the fragmentation and removal of the passive film from the contact surface because of the mechanical damage provoked by the sliding counterparts.[49,51] Then, the OCP of the 316L stainless steel presents a slow decline until reaches a relatively stable value as the tribocorrosion test runs, which is associated with the continuous removal of passive films and the final equilibrium establishment between the mechanical depassivation and electrochemical repassivation.[50,52] Once sliding ceases, a rapid increase in the OCP of the 316L stainless steel is observed as a result of the repassivation process. In the case of four Cr/GLC multilayered films, as a whole, the OCP shows more positive value than the 316L stainless steel, suggesting higher chemical inertness and better corrosion resistance in
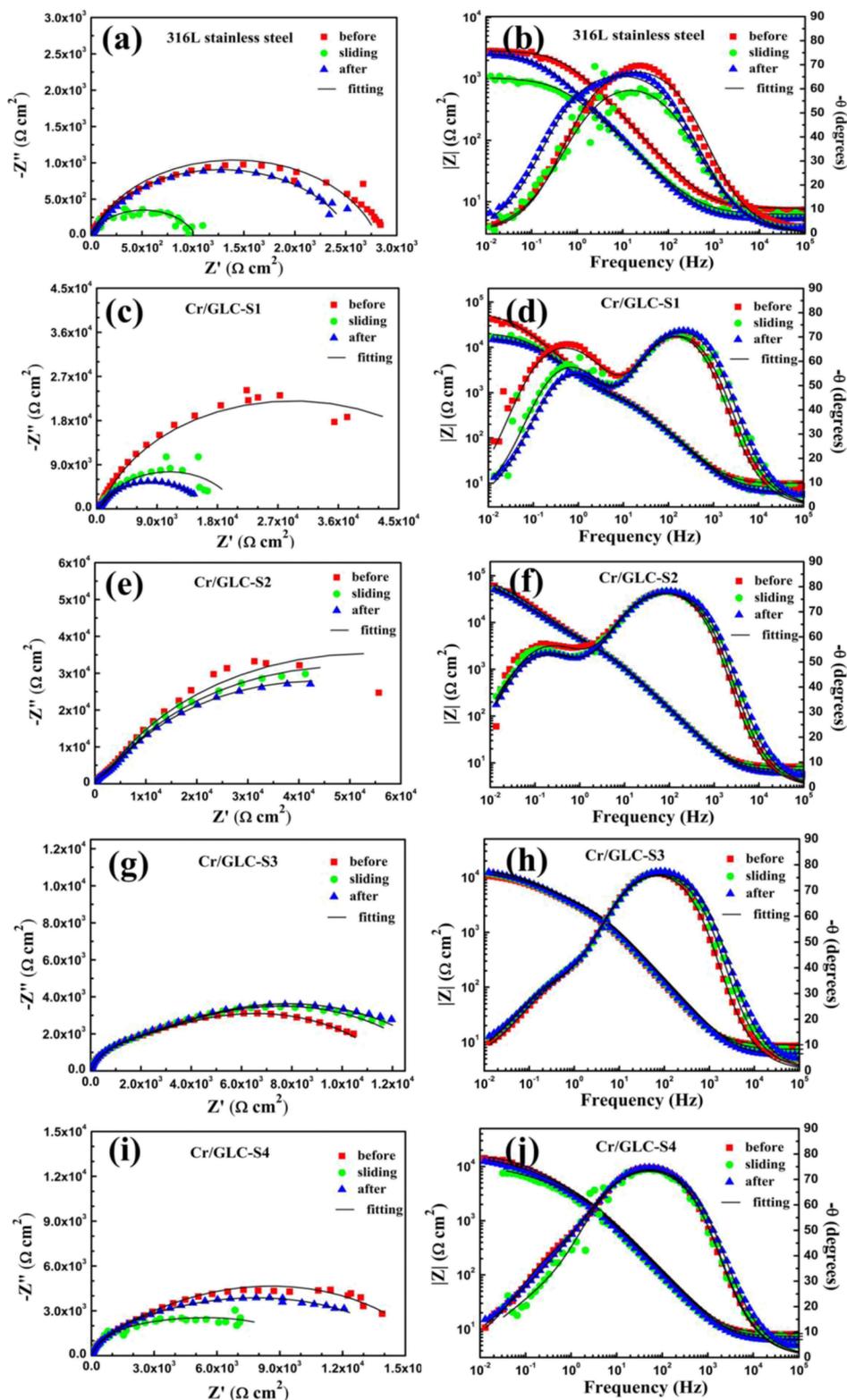
Figure 9. (a,c,e,g,i) Nyquist and (b,d,f,h,j) Bode plots obtained from EIS tests for investigated specimens in artificial seawater before, during, and after sliding.

thermodynamics. Moreover, except for the Cr/GLC-S4 multilayered film, the Cr/GLC multilayered films present a slight potential drop during the whole tribocorrosion process, implying of high capacity to resist mechanical wear in corrosive environments. The activation of Cr/GLC multilayered films during the tribocorrosion test is mainly ascribed to the

expansion and propagation of the micropores and/or microcracks because of the simultaneous action of the corrosive attack and mechanical wear.[51,53]

EIS is a powerful diagnostic technique that is widely employed for the study of coated systems exposed to aggressive chemical environments by measuring the impedance response

to small potential perturbation covering a broad frequency range. Information about the coating defect, the corrosion protectivity, and the corrosion reaction at the coating/substrate interface may be obtained by this technique.[42,54] In this work, EIS is used to assess the variation of electrochemical corrosion resistance of the Cr/GLC multilayered films during mechanical sliding and to evaluate the influence of the modulation period on it.

Figure 9 shows the Nyquist and Bode plots for 316L stainless steel and the four Cr/GLC multilayered films with different modulation periods in artificial seawater before, during, and after sliding. As shown in the Nyquist diagrams, the obvious decrease in the capacitive arc radius is found for tested specimens, especially for 316L stainless steel and Cr/GLC-S1 multilayered film, suggesting that the mechanical sliding accelerates the electrochemical corrosion, which can be further substantiated by the decline of low-frequency impedance limit ($|Z|_f \rightarrow 0$) observed in the Bode plots. At variance with the other Cr/GLC multilayered films, whose corrosion resistance deteriorates after the tribocorrosion test, the corrosion resistances of 316L stainless steel and the Cr/GLC-S4 multilayered film after sliding rebounded appreciably, and this can be rationalized based on the repassivation of the exposed bare metal.[5]

To obtain quantitative result on the corrosion resistance of the investigated specimens, impedance spectra are fitted to reasonable circuit model using the ZSimpWin software. As shown in Figure 9b, the Bode plot of 316L stainless steel presents high-symmetry configuration, corresponding to one time constant, while two time constants are clearly distinguished for four Cr/GLC multilayered films. Therefore, the electronic equivalent circuits shown in Figure 10a,b are
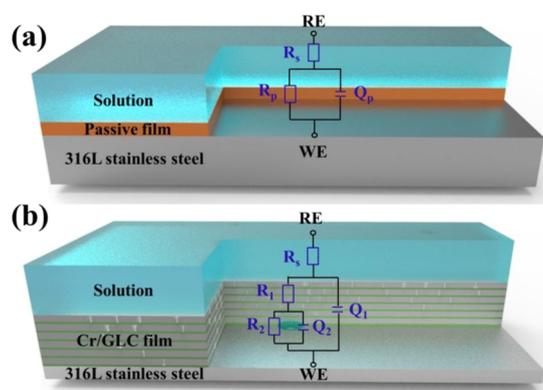
Figure 10. Electronic equivalent circuits employed to simulate the experimental EIS data of (a) 316L stainless steel and (b) Cr/GLC multilayered films.

used, respectively, to simulate the experimental EIS data of 316L stainless steel and the Cr/GLC multilayered films. In the equivalent circuit represented in Figure 10a, commonly known as the Randle circuit, R_s is the solution resistance, Q_p is the constant phase element representing the passive surface capacitance, and R_p is the polarization resistance. The equivalent circuit shown in Figure 10b consists of the solution resistance (R_s) in series with two hierarchical parallel RC configurations, which is typically used to model impedance data of coated systems.[54,55] In this circuit, Q_1 represents the capacitive behavior of the Cr/GLC film, R_1 is the resistance to current flow through the ionic paths and/or structural defects

in the coating, and Q_2 and R_2 correspond to the double capacitance and charge transfer resistance, respectively. Using the above circuit models, the adequate fittings are achieved to the measured impedance data, as shown in Figure 9. The obtained circuit parameter values from the fitting procedures are presented in Figure 11. Clearly, the Cr/GLC multilayered films, independence of the modulation period, significantly improve the corrosion resistance of 316L stainless steel in artificial seawater. For the Cr/GLC multilayered films, the polarization resistance, $R_p = R_1 + R_2$, first increases and then drastically decreases as the modulation period decreases from 1000 to 250 nm. During the tribocorrosion test, the polarization resistance of the Cr/GLC-S1 multilayered film sharply decreases from 5.78×10^4 to 2.08×10^4 Ω cm^2, indicative of degraded corrosion resistance, which is related to the increased porosity left and crack propagation by the mechanical sliding, permitting an easier penetration of the corrosive media into the coating. For the Cr/GLC-S2 multilayered film, a slight decrease from 1.05×10^5 to 9.80×10^4 Ω cm^2 was observed in the polarization resistance when mechanical sliding took place. In the case of other two Cr/GLC multilayered films, no appreciable reduction in the corrosion resistance is found, indicating that the mechanical wear has almost no impact on the corrosion resistance and the corrosion resistance of the two Cr/GLC multilayered films dominates their tribocorrosion performance in artificial seawater.

3.5. Optimization Design for Cr/GLC Films. On the basis of the above analysis, the Cr/GLC-S4 film with the modulation period of 250 nm is optimized by top-layer thickening design: the top GLC layer was thickened to 325 nm. Figure 12 shows the TEM image of the cross section of the optimized Cr/GLC-S5 film, which displays a periodic multilayer structure consisting of dark Cr layers and bright GLC layers. The selected area electron diffraction (SAED) pattern of the GLC layer in the Cr/GLC-S5 film, as shown in the inset of Figure 12, is dispersive and broad, which validates the amorphous nature of the GLC layer.[56−58]

Figure 13a shows the average friction coefficients and wear rates of the Cr/GLC-S5 multilayered film in the tribocorrosion test without and with cathodic protection. As shown, under tribocorrosion condition, the friction coefficient and wear rate of the Cr/GLC-S5 film were 0.046 and 3.17×10^{-7} mm^3/Nm, respectively, which are lower than those of the Cr/GLC-S3 film. Under cathodic protection, the values of the average friction coefficient and wear rate are expected to decrease compared with those in the case of tribocorrosion condition. The wear rate ratio between with and without cathodic protection in the tribocorrosion test is about 82%. Figure 13b presents the wear track morphology on the optimized Cr/GLC-S5 film under tribocorrosion condition. The current evolution curve of the Cr/GLC-S5 film under cathodic protection condition is provided as the Supporting Information in Figure S4. Almost inappreciable wear track and few pitlike corrosion evidence are observed on the wear track, indicating that the optimized Cr/GLC-S5 film presents the excellent tribocorrosion resistance in artificial seawater. As analyzed before, the multilayer structure could prevent the formation of through-coating defects and hinder the sliding-induced crack propagation. Compared with the Cr/GLC-S4 film, the Cr/GLC-S5 film with thickened top layer reveals obviously improved corrosion and wear resistance in artificial seawater, and this manifests that the strategy combining multilayer structure and top-layer thickening is of paramount importance
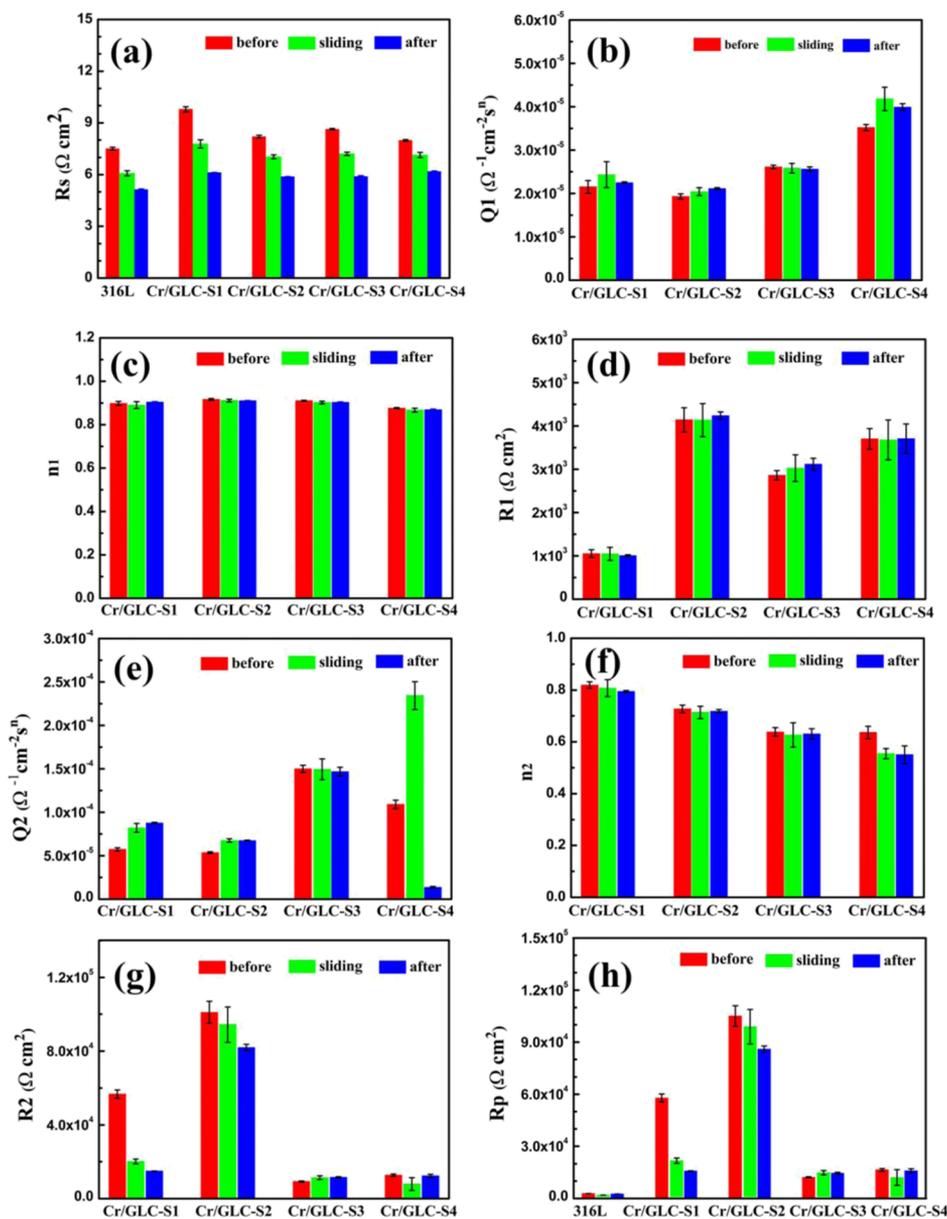
Figure 11. Electrochemical parameters derived from impedance fitting for investigated specimens in artificial seawater before, during, and after sliding. (a) R_s; (b) Q_1; (c) n_1; (d) R_1; (e) Q_2; (f) n_2; (g) R_2; (h) R_p.

to the out-bound tribocorrosion resistance of Cr/GLC films in artificial seawater. The typical friction coefficient curves of the Cr/GLC-S5 multilayered film and uncoated 316L SS can be found in the Supporting Information (Figure S5).

Figure 14 presents the Nyquist and Bode plots of the Cr/GLC-S5 multilayered film in artificial seawater before, during, and after the tribocorrosion test, and corresponding equivalent circuit parameters are listed in Table 4. Obviously, the Cr/GLC-S5 multilayered film exhibits significantly higher corrosion resistance as compared to other four Cr/GLC multilayered films, suggesting that the top-layer thickening is an effective way to improve the anticorrosion property of the Cr/GLC multilayered film. Furthermore, similar to the Cr/GLC-S3 and Cr/GLC-S4 multilayered film, the corrosion resistances of the Cr/GLC-S5 multilayered film during and after the tribocorrosion test are comparable to that before mechanical sliding, reflecting superior triboelectrochemical property.

Sun et al.[59] stated that the high energy ion could pass through the individual layer of multilayer film with a small modulation period, accelerating the corrosion process. To evaluate the influence of the individual layer thickness on the vacancy type structural defect of the Cr/GLC multilayered films, Mott−Schottky analysis was conducted. This method utilizes the applied potential dependency of the interfacial capacitance to extract information about the doping type and level of the semiconductor material.[60] If the semiconductor−electrolyte system obeys Mott−Schottky behavior, the square of reciprocal space-charge capacitance ($1/C_{sc}^2$) will show linear dependence on the applied potential (E). The sign and the value of the linear region slope are representative of the doping type and of the carrier concentration (N_q), respectively. The numerical value of N_q can be calculated using the following Mott−Schottky equation:[61,62]
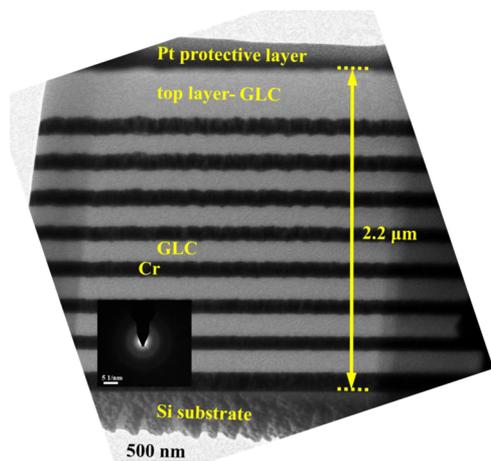
Figure 12. Cross-sectional TEM micrographs of the Cr/GLC-S5 multilayered film and the corresponding SAED pattern of the carbon layer.
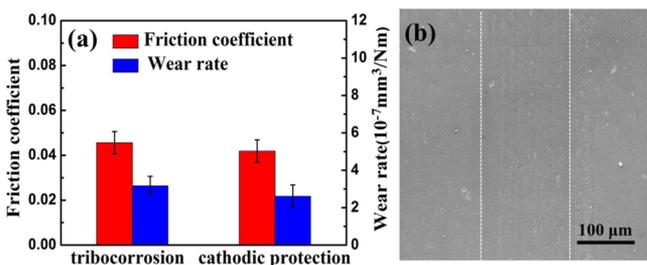
Figure 13. (a) Average friction coefficients, wear rates of the Cr/GLC-S5 multilayered film; (b) wear track morphology of the Cr/GLC-S5 multilayered film under tribocorrosion condition.

$$\frac{1}{C_{sc}^{2}} = \frac{2}{\varepsilon_r \varepsilon_0 q N_q}\left(E - E_{fb} - \frac{kT}{q}\right) \tag{4}$$

where ε_r is the dielectric constant of the GLC top layer, ε_0 is the vacuum permittivity, q is the elementary charge (+e for electrons and −e for holes), N_q is the carrier concentration (N_d for donors and N_a for acceptors), E_{fb} is the flat band potential, k is the Boltzmann constant, and T is the absolute temperature. In this work, the space-charge capacitance (C_{sc}) was assumed to be equal to the interfacial capacitance (C) at sufficiently high frequencies.

Figure 15 shows the Mott−Schottky plots of the Cr/GLC-S4 and Cr/GLC-S5 multilayered films in artificial seawater, which display good linear relationship between $1/C_{sc}^{2}$ and E with

positive slopes, indicating n-type semiconductor character of the GLC top layer. Moreover, the slope of the Cr/GLC-S5 multilayered film is obviously higher than that of the Cr/GLC-S4 multilayered film, indicative of reduced carrier concentration in the thickened GLC top layer. The low carrier concentration signifies decreased vacancy type structural defect, which is conducive to restrain the penetration of corrosive ion and, consequently, to improve the corrosion resistance.

4. CONCLUSIONS

To improve the tribocorrosion resistance of Fe-based tribocomponents exposed to marine environments, Cr/GLC multilayered films with different modulation periods were deposited onto 316L stainless steel by dc magnetron sputtering. After the microstructural characterization and mechanical testing, the electrochemical corrosion and tribocorrosion behaviors of Cr/GLC films were systematically investigated in artificial seawater, and the main conclusions were summarized as follows:

(1) The as-deposited Cr/GLC multilayered films consisted of cyclical Cr and GLC layer. The variation of modulation period did not change the atomic bond structure of sp^2 content in the GLC layer. The hardness and the H^3/E^2 value of the Cr/GLC multilayered films increased with decreasing modulation period, while the elastic modulus increased from S1 to S2 with decreasing modulation period and then leveled off around 193 GPa as the modulation period further reduced.

(2) The Cr/GLC multilayered films presented the different tribocorrosion resistance dependence on the modulation period. For the Cr/GLC S1−S3 multilayered films, the friction coefficient and wear rate decreased with decreasing modulation period from 1000 to 333 nm, while the Cr/GLC-S4 film with 250 nm modulation period presents premature tribocorrosion failure.

(3) The corrosion resistance of Cr/GLC multilayered films was improved with decreasing modulation period from 1000 to 500 nm and then abruptly declined as the modulation period further decreased to 333 and 250 nm. In contrast to the Cr/GLC-S1 and Cr/GLC-S2 multilayered films, the mechanical wear had no deteriorating effect on the corrosion resistance of the Cr/GLC-S3 and Cr/GLC-S4 multilayered films.

(4) The optimized Cr/GLC-S4 multilayered film with designed thickened top layer presented the excellent corrosion and tribocorrosion resistance in artificial seawater, suggesting that the combined multilayer
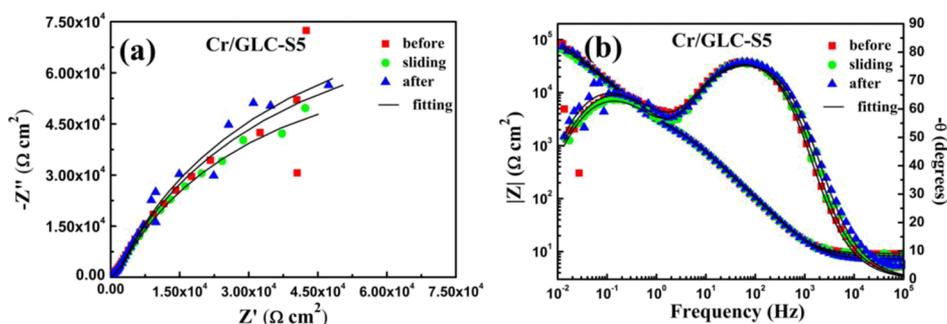
Figure 14. (a) Nyquist and (b) Bode plots obtained from EIS tests for the Cr/GLC-S5 multilayered film in artificial seawater before, during, and after sliding.

Table 4. Equivalent Circuit Parameters Derived from Impedance Fitting for the Cr/GLC-S5 Multilayered Film in Artificial Seawater before, during, and after Sliding

status	before sliding	during sliding	after sliding
R_s (Ω cm^2)	9.11 ± 0.13	8.22 ± 0.12	7.09 ± 0.08
Q_1 (Ω^{-1} cm^{-2} s^n)	$(2.89 \pm 0.14) \times 10^{-5}$	$(2.97 \pm 0.14) \times 10^{-5}$	$(3.03 \pm 0.10) \times 10^{-5}$
n_1	0.909 ± 0.007	0.900 ± 0.007	0.894 ± 0.004
R_1 (Ω cm^2)	$(3.16 \pm 0.34) \times 10^3$	$(3.15 \pm 0.32) \times 10^3$	$(3.35 \pm 0.22) \times 10^3$
Q_2 (Ω^{-1} cm^{-2} s^n)	$(5.73 \pm 0.17) \times 10^{-5}$	$(6.60 \pm 0.19) \times 10^{-5}$	$(6.14 \pm 0.13) \times 10^{-5}$
n_2	0.782 ± 0.020	0.775 ± 0.021	0.809 ± 0.014
R_2 (Ω cm^2)	$(1.73 \pm 0.20) \times 10^5$	$(1.47 \pm 0.17) \times 10^5$	$(1.80 \pm 0.15) \times 10^5$
R_p (Ω cm^2)	$(1.76 \pm 0.20) \times 10^5$	$(1.50 \pm 0.17) \times 10^5$	$(1.83 \pm 0.15) \times 10^5$
χ^2	3.39×10^{-3}	3.55×10^{-3}	1.68×10^{-3}
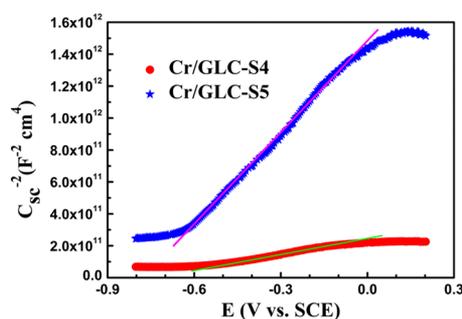
Figure 15. Mott−Schottky plots of the Cr/GLC-S4 and Cr/GLC-S5 multilayered films in artificial seawater.

structure and top-layer thickening design was an effective strategy to improve the tribocorrosion performance of GLC films.

ASSOCIATED CONTENT

⊕ Supporting Information

The Supporting Information is available free of charge on the ACS Publications website at DOI: 10.1021/acsami.8b00628.

> Potentiodynamic polarization curves and current evolution curves of Cr/GLC multilayered films; Raman spectra; and current evolution curves, friction coefficients, and surface morphologies of wear tracks of the Cr/GLC-S5 multilayered film and uncoated 316L SS (PDF)

AUTHOR INFORMATION

Corresponding Authors

*E-mail: kepl@nimte.ac.cn. Phone: 86-574-86685170. Fax: 86-574-86685159 (P.K.).

*E-mail: aywang@nimte.ac.cn. Phone: 86-574-86685170. Fax: 86-574-86685159 (A.W).

ORCID ⊙

Lei Li: 0000-0002-9450-1628

Xiaowei Li: 0000-0002-7042-2546

Aiying Wang: 0000-0003-2938-5437

Author Contributions

§L.L. and L.-L.L. contributed to this work equally.

Notes

The authors declare no competing financial interest.

REFERENCES

(1) Wood, R. J. K. Marine wear and tribocorrosion. *Wear* **2017**, *376−377*, 893−910.

(2) Costa, R. P. C.; Lima-Oliveira, D. A.; Marciano, F. R.; Lobo, A. O.; Corat, E. J.; Trava-Airoldi, V. J. Comparative study of the tribological behavior under hybrid lubrication of diamond-like carbon films with different adhesion interfaces. *Appl. Surf. Sci.* **2013**, *285*, 645−648.

(3) Hirani, H.; Goilkar, S. S. Formation of transfer layer and its effect on friction and wear of carbon−graphite face seal under dry, water and steam environments. *Wear* **2009**, *266*, 1141−1154.

(4) Kok, Y. N.; Akid, R.; Hovsepian, P. E. Tribocorrosion testing of stainless steel (SS) and PVD coated SS using a modified scanning reference electrode technique. *Wear* **2005**, *259*, 1472−1481.

(5) Mischler, S. Triboelectrochemical techniques and interpretation methods in tribocorrosion: A comparative evaluation. *Tribol. Int.* **2008**, *41*, 573−583.

(6) Wood, R. J. K. Erosion−corrosion interactions and their effect on marine and offshore materials. *Wear* **2006**, *261*, 1012−1023.

(7) Wu, P.-Q.; Celis, J.-P. Electrochemical noise measurements on stainless steel during corrosion−wear in sliding contacts. *Wear* **2004**, *256*, 480−490.

(8) Landolt, D.; Mischler, S.; Stemp, M. Electrochemical methods in tribocorrosion: a critical appraisal. *Electrochim. Acta* **2001**, *46*, 3913−3929.

(9) Zheng, J.; Chen, H.; Qiao, L.; Lin, M.; Jiang, L.; Che, S.; Hu, Y. Double coating protection of Nd-Fe-B magnets: Intergranular phosphating treatment and copper plating. *J. Magn. Magn. Mater.* **2014**, *371*, 1−4.

(10) Peña-Parás, L.; Maldonado-Cortés, D.; García, P.; Irigoyen, M.; Taha-Tijerina, J.; Guerra, J. Tribological performance of halloysite clay nanotubes as green lubricant additives. *Wear* **2017**, *376−377*, 885−892.

(11) von der Ohe, C. B.; Johnsen, R.; Espallargas, N. Multi-degradation behavior of austenitic and super duplex stainless steel − The effect of 4-point static and cyclic bending applied to a simulated seawater tribocorrosion system. *Wear* **2012**, *288*, 39−53.

(12) Zhang, T. F.; Deng, Q. Y.; Liu, B.; Wu, B. J.; Jing, F. J.; Leng, Y. X.; Huang, N. Wear and corrosion properties of diamond like carbon (DLC) coating on stainless steel, CoCrMo and Ti6Al4V substrates. *Surf. Coat. Technol.* **2015**, *273*, 12−19.

(13) Totolin, V.; Pejaković, V.; Csanyi, T.; Hekele, O.; Huber, M.; Ripoll, M. R. Surface engineering of Ti6Al4V surfaces for enhanced tribocorrosion performance in artificial seawater. *Mater. Des.* **2016**, *104*, 10−18.

(14) Huang, J.; Wang, L.; Liu, B.; Wan, S.; Xue, Q. In vitro evaluation of the tribological response of Mo-doped graphite-like carbon film in different biological media. *ACS Appl. Mater. Interfaces* **2015**, *7*, 2772−2783.

(15) Guan, X.; Wang, L. The Tribological Performances of Multilayer Graphite-Like Carbon (GLC) Coatings Sliding Against Polymers for Mechanical Seals in Water Environments. *Tribol. Lett.* 2012, 47, 67−78.

(16) Li, L.; Bai, W.; Wang, X.; Gu, C.; Jin, G.; Tu, J. Mechanical Properties, in Vitro and in Vivo Biocompatibility of a-C/a-C: Ti Nanomultilayer Films on Ti6Al4V Alloy as Medical Implants. *ACS Appl. Mater. Interfaces* 2017, 9, 15933.

(17) Voevodin, A. A.; Donley, M. S.; Zabinski, J. S.; Bultman, J. E. Mechanical and tribological properties of diamond-like carbon coatings prepared by pulsed laser deposition. *Surf. Coat. Technol.* 1995, 76−77, 534−539.

(18) Wang, Y.; Li, H.; Ji, L.; Liu, X.; Wu, Y.; Lv, Y.; Fu, Y.; Zhou, H.; Chen, J. Synthesis and characterization of titanium-containing graphite-like carbon films with low internal stress and superior tribological properties. *J. Phys. D: Appl. Phys.* 2012, 45, 295301.

(19) Cui, M.; Pu, J.; Liang, J.; Wang, L.; Zhang, G.; Xue, Q. Corrosion and tribocorrosion performance of multilayer diamond-like carbon film in NaCl solution. *RSC Adv.* 2015, 5, 104829−104840.

(20) He, X.; Li, W.; Li, H. Diamond-like carbon film synthesized by ion beam assisted deposition and its tribological properties. *J. Vac. Sci. Technol., A* 1996, 14, 2039−2047.

(21) Kiuru, M.; Alakoski, E.; Tiainen, V.-M.; Lappalainen, R.; Anttila, A. Tantalum as a buffer layer in diamond-like carbon coated artificial hip joints. *J. Biomed. Mater. Res., Part B* 2003, 66, 425−428.

(22) Wang, Y.; Wang, L.; Xue, Q. Controlling wear failure of graphite-like carbon film in aqueous environment: Two feasible approaches. *Appl. Surf. Sci.* 2011, 257, 4370−4376.

(23) Bai, W. Q.; Li, L. L.; Xie, Y. J.; Liu, D. G.; Wang, X. L.; Jin, G.; Tu, J. P. Corrosion and tribocorrosion performance of M (M Ta, Ti) doped amorphous carbon multilayers in Hank's solution. *Surf. Coat. Technol.* 2016, 305, 11−22.

(24) Zhang, W.; Tanaka, A.; Xu, B. S.; Koga, Y. Study on the diamond-like carbon multilayer films for tribological application. *Diamond Relat. Mater.* 2005, 14, 1361−1367.

(25) Bai, W. Q.; Xie, Y. J.; Li, L. L.; Wang, X. L.; Gu, C. D.; Tu, J. P. Tribological and corrosion behaviors of Zr-doped graphite-like carbon nanostructured coatings on Ti6Al4V alloy. *Surf. Coat. Technol.* 2017, 320, 235−239.

(26) Ma, F.; Li, J.; Zeng, Z.; Gao, Y. Structural, mechanical and tribocorrosion behaviour in artificial seawater of CrN/AlN nano-multilayer coatings on F690 steel substrates. *Appl. Surf. Sci.* 2018, 428, 404−414.

(27) Mendizabal, L.; Lopez, A.; Bayón, R.; Herrero-Fernandez, P.; Barriga, J.; Gonzalez, J. J. Tribocorrosion response in biological environments of multilayer TaN films deposited by HPPMS. *Surf. Coat. Technol.* 2016, 295, 60−69.

(28) Wang, Y.; Pu, J.; Wang, J.; Li, J.; Chen, J.; Xue, Q. Interlayer design for the graphite-like carbon film with high load-bearing capacity under sliding-friction condition in water. *Appl. Surf. Sci.* 2014, 311, 816−824.

(29) Stallard, J.; Mercs, D.; Jarratt, M.; Teer, D. G.; Shipway, P. H. A study of the tribological behaviour of three carbon-based coatings, tested in air, water and oil environments at high loads. *Surf. Coat. Technol.* 2004, 177−178, 545−551.

(30) Wang, J.; Yan, F.; Xue, Q. Tribological behaviors of some polymeric materials in sea water. *Sci. Bull.* 2009, 54, 4541−4548.

(31) Qi, J.; Wang, L.; Wang, Y.; Pu, J.; Yan, F.; Xue, Q. The tribological performance of selected solid lubricant films in sand-dust environments. *Wear* 2011, 271, 899−910.

(32) Chen, X.; Peng, Z.; Yu, X.; Fu, Z.; Yue, W.; Wang, C. Microstructure and tribological performance of self-lubricating diamond/tetrahedral amorphous carbon composite film. *Appl. Surf. Sci.* 2011, 257, 3180−3186.

(33) Ferrari, A. C.; Robertson, J. Interpretation of Raman spectra of disordered and amorphous carbon. *Phys. Rev. B: Condens. Matter Mater. Phys.* 2000, 61, 14095−14107.

(34) Ipaz, L.; Caicedo, J. C.; Esteve, J.; Espinoza-Beltran, F. J.; Zambrano, G. Improvement of mechanical and tribological properties

(35) Li, C.-L.; Wu, F.-B.; Lee, J.-W.; Tsai, Y.-Z.; Chang, L.-C. Characteristics of Cr$_2$N/Cu multilayered thin films with different bilayer thickness. *Surf. Coat. Technol.* 2009, 204, 941−946.

(36) Xu, Z.; Sun, H.; Leng, Y. X.; Li, X.; Yang, W.; Huang, N. Effect of modulation periods on the microstructure and mechanical properties of DLC/TiC multilayer films deposited by filtered cathodic vacuum arc method. *Appl. Surf. Sci.* 2015, 328, 319−324.

(37) Koehler, J. S. Attempt to Design a Strong Solid. *Phys. Rev. B: Solid State* 1970, 2, 547−551.

(38) Neumann, J. P. On the occurrence of substitutional and triple defects in intermetallic phases with the B2 structure. *Acta Metall.* 1980, 28, 1165−1170.

(39) Kim, G. S.; Lee, S. Y.; Hahn, J. H.; Lee, S. Y. Synthesis of CrN/AlN superlattice coatings using closed-field unbalanced magnetron sputtering process. *Surf. Coat. Technol.* 2003, 171, 91−95.

(40) Shum, P. W.; Zhou, Z. F.; Li, K. Y.; Chan, C. Y. Mechanical and tribological properties of amorphous carbon films deposited on implanted steel substrates. *Thin Solid Films* 2004, 458, 203−211.

(41) Zhang, B.; Wang, J.; Yan, F. Load-dependent tribocorrosion behaviour of nickel-aluminium bronze in artificial seawater. *Corros. Sci.* 2018, 131, 252−263.

(42) Ahn, S. H.; Lee, J. H.; Kim, H. G.; Kim, J. G. A study on the quantitative determination of through-coating porosity in PVD-grown coatings. *Appl. Surf. Sci.* 2004, 233, 105−114.

(43) Mathew, M. T.; Ariza, E.; Rocha, L. A.; Vaz, F.; Fernandes, A. C.; Stack, M. M. Tribocorrosion behaviour of TiC$_x$O$_y$ thin films in bio-fluids. *Electrochim. Acta* 2010, 56, 929−937.

(44) Sadiq, K.; Black, R. A.; Stack, M. M. Bio-tribocorrosion mechanisms in orthopaedic devices: Mapping the micro-abrasion−corrosion behaviour of a simulated CoCrMo hip replacement in calf serum solution. *Wear* 2014, 316, 58−69.

(45) Sadiq, K.; Stack, M. M.; Black, R. A. Wear mapping of CoCrMo alloy in simulated bio-tribocorrosion conditions of a hip prosthesis bearing in calf serum solution. *Mater. Sci. Eng., C* 2015, 49, 452−462.

(46) Chen, J.; Wang, J.; Yan, F.; Zhang, Q.; Li, Q.-a. Effect of applied potential on the tribocorrosion behaviors of Monel K500 alloy in artificial seawater. *Tribol. Int.* 2015, 81, 1−8.

(47) Gao, S.; Dong, C.; Luo, H.; Xiao, K.; Pan, X.; Li, X. Scanning electrochemical microscopy study on the electrochemical behavior of CrN film formed on 304 stainless steel by magnetron sputtering. *Electrochim. Acta* 2013, 114, 233−241.

(48) Dorner-Reisel, A.; Schürer, C.; Irmer, G.; Müller, E. Electro-chemical corrosion behaviour of uncoated and DLC coated medical grade Co28Cr6Mo. *Surf. Coat. Technol.* 2004, 177−178, 830−837.

(49) Bayón, R.; Igartua, A.; González, J. J.; de Gopegui, U. R. Influence of the carbon content on the corrosion and tribocorrosion performance of Ti-DLC coatings for biomedical alloys. *Tribol. Int.* 2015, 88, 115−125.

(50) Yan, Y.; Neville, A.; Dowson, D. Tribo-corrosion properties of cobalt-based medical implant alloys in simulated biological environ-ments. *Wear* 2007, 263, 1105−1111.

(51) Liu, J.; Wang, X.; Wu, B. J.; Zhang, T. F.; Leng, Y. X.; Huang, N. Tribocorrosion behavior of DLC-coated CoCrMo alloy in simulated biological environment. *Vacuum* 2013, 92, 39−43.

(52) Yan, Y.; Neville, A.; Dowson, D.; Williams, S.; Fisher, J. Effect of metallic nanoparticles on the biotribocorrosion behaviour of Metal-on-Metal hip prostheses. *Wear* 2009, 267, 683−688.

(53) Manhabosco, T. M.; Barboza, A. P. M.; Batista, R. J. C.; Neves, B. R. A.; Müller, I. L. Corrosion, wear and wear−corrosion behavior of graphite-like a -C: H films deposited on bare and nitrided titanium alloy. *Diamond Relat. Mater.* 2013, 31, 58−64.

(54) Liu, C.; Bi, Q.; Leyland, A.; Matthews, A. An electrochemical impedance spectroscopy study of the corrosion behaviour of PVD coated steels in 0.5 N NaCl aqueous solution: Part II. : EIS interpretation of corrosion behaviour. *Corros. Sci.* 2003, 45, 1257−1273.

in steel surfaces by using titanium−aluminum/titanium−aluminum nitride multilayered system. *Appl. Surf. Sci.* 2012, 258, 3805−3814.

(55) Grips, V. K. W.; Selvi, V. E.; Barshilia, H. C.; Rajam, K. S. Effect of electroless nickel interlayer on the electrochemical behavior of single layer CrN, TiN, TiAlN coatings and nanolayered TiAlN/CrN multilayer coatings prepared by reactive dc magnetron sputtering. *Electrochim. Acta* **2006**, *51*, 3461−3468.

(56) Hadinata, S.-S.; Lee, M.-T.; Pan, S.-J.; Tsai, W.-T.; Tai, C.-Y.; Shih, C.-F. Electrochemical performances of diamond-like carbon coatings on carbon steel, stainless steel, and brass. *Thin Solid Films* **2013**, *529*, 412−416.

(57) Rejowski, E. D.; de Oliveira, M. C. L.; Antunes, R. A.; Pillis, M. F. Structural Characterization and Corrosion Stability of a Si-Doped DLC Coating Applied on Cylinder Liner. *J. Mater. Eng. Perform.* **2014**, *23*, 3926−3933.

(58) Zhu, W.; Nie, C. Y.; Ran, C. H.; Jin, Y. D.; Zhao, Y. Study on Electrochemical Corrosion Behavior Comparison between DLC and TiN Coatings under Different Corrosive Environment. *Adv. Mater. Res.* **2013**, *750−752*, 1977−1981.

(59) Sun, T.; Wang, L.; Yu, Y.; Wang, Y.; Wang, X.; Tang, B. TiN/ZrO$_2$ multilayers synthesized on GCr15 bearing steel using plasma immersion ion implantation and deposition. *Surf. Coat. Technol.* **2007**, *201*, 6615−6618.

(60) Morrison, S. R. *Electrochemistry at Semiconductor and Oxidized Metal Electrodes*; Springer, 1980.

(61) Ge, H.-H.; Xu, X.-M.; Zhao, L.; Song, F.; Shen, J.; Zhou, G.-D. Semiconducting behavior of passive film formed on stainless steel in borate buffer solution containing sulfide. *J. Appl. Electrochem.* **2011**, *41*, 519−525.

(62) Liu, L.; Xu, J.; Jiang, S. Nanocrystalline β-Ta Coating Enhances the Longevity and Bioactivity of Medical Titanium Alloys. *Metals* **2016**, *6*, 221.